AGU PUBLICATIONS

JGR

Journal of Geophysical Research: Earth Surface

RESEARCH ARTICLE
10.1002/2016JF003869

Key Points:
- Firn aquifers represent a total area of 21,900 km^2 when inferred from airborne radar data collected between 2010 and 2014
- Water table interannual variations imply filling and drainage
- Water flows in the firn aquifer under low hydraulic gradients following local surface topography

Supporting Information:
- Figures S1 and S2

Correspondence to:
C. Miège,
clement.miege@geog.utah.edu

Citation:
Miège, C., et al. (2016), Spatial extent and temporal variability of Greenland firn aquifers detected by ground and airborne radars, *J. Geophys. Res. Earth Surf.*, *121*, 2381–2398, doi:10.1002/2016JF003869.

Received 1 MAR 2016
Accepted 14 NOV 2016
Accepted article online 15 NOV 2016
Published online 20 DEC 2016

Spatial extent and temporal variability of Greenland firn aquifers detected by ground and airborne radars

Clément Miège[1], Richard R. Forster[1], Ludovic Brucker[2,3], Lora S. Koenig[4], D. Kip Solomon[5], John D. Paden[6], Jason E. Box[7], Evan W. Burgess[1], Julie Z. Miller[1,8], Laura McNerney[1], Noah Brautigam[1], Robert S. Fausto[7], and Sivaprasad Gogineni[6]

[1]Department of Geography, University of Utah, Salt Lake City, Utah, USA, [2]Cryospheric Sciences Laboratory, Code 615, NASA Goddard Space Flight Center, Greenbelt, Maryland, USA, [3]Universities Space Research Association, Goddard Earth Sciences Technology and Research Studies and Investigations, Columbia, Maryland, USA, [4]National Snow and Ice Data Center, Cooperative Institute for Research in Environmental Sciences, University of Colorado Boulder, Boulder, Colorado, USA, [5]Department of Geology and Geophysics, University of Utah, Salt Lake City, Utah, USA, [6]Center for Remote Sensing of Ice Sheets, University of Kansas, Lawrence, Kansas, USA, [7]Geological Survey of Denmark and Greenland (GEUS), Copenhagen, Denmark, [8]Byrd Climate and Research Center, Ohio State University, Columbus, Ohio, USA

Abstract We document the existence of widespread firn aquifers in an elevation range of ~1200–2000 m, in the high snow-accumulation regions of the Greenland ice sheet. We use NASA Operation IceBridge accumulation radar data from five campaigns (2010–2014) to estimate a firn-aquifer total extent of 21,900 km^2. We investigate two locations in Southeast Greenland, where repeated radar profiles allow mapping of aquifer-extent and water table variations. In the upper part of Helheim Glacier the water table rises in spring following above-average summer melt, showing the direct firn-aquifer response to surface meltwater production changes. After spring 2012, a drainage of the firn-aquifer lower margin (5 km) is inferred from both 750 MHz accumulation radar and 195 MHz multicoherent radar depth sounder data. For 2011–2014, we use a ground-penetrating radar profile located at our Ridgeline field site and find a spatially stable aquifer with a water table fluctuating less than 2.5 m vertically. When combining radar data with surface topography, we find that the upper elevation edge of firn aquifers is located directly downstream of locally high surface slopes. Using a steady state 2-D groundwater flow model, water is simulated to flow laterally in an unconfined aquifer, topographically driven by ice sheet surface undulations until the water encounters crevasses. Simulations suggest that local flow cells form within the Helheim aquifer, allowing water to discharge in the firn at the steep-to-flat transitions of surface topography. Supported by visible imagery, we infer that water drains into crevasses, but its volume and rate remain unconstrained.

1. Introduction

Mass loss of the Greenland ice sheet has been accelerating since the 1990s [*Rignot et al*., 2011], and in recent years (2009–2012), about 85% of its rate of increase were due to increased surface melt and subsequent runoff [*Enderlin et al*., 2014]. Greenland surface melt extent and duration have increased over the last decade, in response to increased advection of warm air from the south during summers [e.g., *Tedesco et al*., 2013]. Surface melt is not only occurring in the lower elevation margins of the ice sheet but also migrating toward the ice sheet interior, causing a reduction of the dry-snow zone and an expansion of the percolation zone [*McGrath et al*., 2013]. Widespread firn aquifers have been detected in high accumulation regions (1.2 m w.e. yr^{-1}, water equivalent, in average) of the ice sheet percolation zone [*Forster et al*., 2014]. In these regions, firn aquifers retain water for at least several years, storing a substantial amount of water responsible of heating the firn and delaying runoff [*Forster et al*., 2014; *Kuipers Munneke et al*., 2014]. Their impacts on the ice sheet are numerous, including firn densification, alteration of the ice thermal state, and water input from the aquifer into the englacial hydrology system, which has the potential to affect ice dynamics and Greenland's contribution to sea level rise [*Forster et al*., 2014; *Koenig et al*., 2014].

This work extends previous firn-aquifer studies within the Greenland ice sheet, outlined in section 2 below [*Forster et al*., 2014; *Koenig et al*., 2014; *Kuipers Munneke et al*., 2014], focusing on mapping firn-aquifer extent and investigating short-term temporal evolution between 2010 and 2014 using a combination of airborne radar and lidar data, together with ground observations (radar and firn cores). We first provide background

information on water storage systems on glaciers and ice sheets including water percolation and lateral flow within the firn. We then present a map of the Greenland firn-aquifer extent and depth to water using 5 years of airborne radar data. We investigate annual temporal evolution of the water table over repeated airborne and ground tracks between 2010 and 2014. Finally, we simulate steady state 2-D lateral flow within the firn aquifer and reveal local flow cells due to local surface undulation in the topography.

2. Background

The downward percolation of meltwater into the snow and firn is a nonuniform process in space and time that accelerates snow metamorphism [e.g., *Colbeck*, 1975; *Raymond and Tusima*, 1979]. Water generally flows downward due to gravity, although some water can be retained either in a liquid form in the temperate (0°C) snow/firn microstructure due to surface tension (capillary forces) or by refreezing into a snow/firn layer below 0°C, generating ice lenses. Cold-room experiments by *Coléou and Lesaffre* [1998] suggested that capillary forces hold less than 10% of water in the pore volume of 0°C seasonal snow and that holding capacity decreases with depth and increasing snow/firn density. In their experiment, a water-saturated layer was found at the bottom of each snow sample, with a bulk density of 900–950 kg m^{-3}; this suggests that substantial water retention is possible in natural snowpacks.

The presence of meltwater storage in the firn is well documented for mountain glaciers [e.g., *Fountain and Walder*, 1998; *Jansson et al*., 2003], and a few examples include Vernagtferner; Oetztal Alps [*Oerter and Moser*, 1982]; South Cascade Glacier, USA [*Fountain*, 1989]; and Storglaciären in northern Sweden [*Schneider*, 1999; *Schneider and Jansson*, 2004]. For these last two glaciers, the water in the aquifer seems to be present mainly in the melt season. Drainage from the aquifer is reported for South Cascade by late November [*Fountain*, 1996], and only a small amount of water (irreducible water saturation) is observed to persist by late winter in Storglaciären [*Jansson et al*., 2003]. In Arctic settings, perennial (>1 year) firn water storage is observed within the Holtedahlfonna ice field, Svalbard [*Christianson et al*., 2015]. The depth to the water table depends on elevation, surface slope, and glacier topography and ranges between 0 m and 40 m [*Fountain and Walder*, 1998; *Christianson et al*., 2015]. Despite some variations in depth to the water table and storage time scale, firn aquifers show relatively similar hydraulic characteristics, reflecting a similar seasonal snow grain metamorphism rate in response to water input [*Fountain and Walder*, 1998]. Firn hydraulic conductivity values range from 1 to 5×10^{-5} m s^{-1} with an average porosity of 0.15 [*Fountain and Walder*, 1998]. Aquifer responds to surface meltwater input, and percolation vertical velocities are found to range from 0.12 to 0.35 m h^{-1} for an isothermal firn column, equivalent to ~1–3.5 days to transfer water from the surface to the water table at 10 m depth [*Schneider*, 1999]. In the absence of local sinks, water would flow laterally under hydraulic gradients, following the glacier slope. *Jansson et al*. [2003] found that the firn-aquifer thickness is related to the hydraulic gradient (water table slope) and the efficiency of the englacial network in allowing water to exit the glacier system. The water can eventually drain into nearby crevasses or moulins [*Fountain and Walder*, 1998].

These previous studies provide important observations for understanding the larger firn aquifers observed within the Greenland ice sheet. In the ice sheet firn, stored water exists in regions with moderate to strong summer surface melt and high snow accumulation [*Forster et al*., 2014; *Kuipers Munneke et al*., 2014]. Sufficient early autumn snowfall insulates the firn from the winter surface temperatures, preserving pore space at depth to allow retention and storage of additional meltwater [*Kuipers Munneke et al*., 2014]. In the ice sheet percolation zone, the firn stratigraphy is heterogeneous and characterized by ice lenses (horizontal) and ice columns/pipes (vertical) [e.g., *Benson*, 1962]. Ice inclusions offer preferential pathways for meltwater to travel, changing firn physical properties through a complicated meltwater routing system [*Pfeffer and Humphrey*, 1996; *Humphrey et al*., 2012; *Machguth et al*., 2016]. At greater depths (>10 m), water-saturated layers can persist in the firn over the winter [*Humphrey et al*., 2012], similar to groundwater aquifers [*Forster et al*., 2014]. The Greenland firn aquifer is usually present in a 10–20 km wide band that rings the southeast and south ice sheet perimeter and has smaller average slopes (less than 1°) [*Forster et al*., 2014]. Assuming a similar hydraulic conductivity value as glaciers and weak hydraulic gradients, it would take years for water at the high-elevation end of the water-saturated firn layer to exit the firn via the englacial hydrology system [*Humphrey et al*., 2012].

3. Study Site

Surface-based measurements were made on the southeast part of the ice sheet (66.18°N, 39.04°W; ~1560 m), 50 km west from Sermilik Fjord on a ridgeline south of Helheim Glacier, named "Ridgeline Site" in the following (Figure 1). Fifteen kilometers west of our field site the ice thickness is 1000 m, according to observations from the Operation IceBridge (OIB) 2012 Multichannel Coherent Radar Depth Sounder (MCoRDS) [*Leuschen et al*., 2014b]. Our field site was initially chosen for firn-core extraction to verify the simulated high accumulation rates (1.44 ± 0.30 m w.e. yr^{-1} [*Burgess et al*., 2010] and 1.67 ± 0.29 m w.e. yr^{-1} [*Fettweis et al*., 2013]) and large interannual variations in the region [*Miège et al*., 2013]. At this location, melt averages 0.73 ± 0.17 m w.e. yr^{-1} over the 1979–2014 period, are simulated by the Model Atmospheric Regional (MAR) with a substantial increase over the last decade [*Fettweis et al*., 2013]. For the 2010–2014 period, summer melt in 2011 (0.73 m w.e.) was within the 1979–2014 average, whereas the summers of 2010 and 2012 were characterized by important melting with 1.04 and 1.18 m w.e. yr^{-1}, respectively (Figure 1c) [*Fettweis et al*., 2013]. Our field work at this site was conducted in April to early May 2013–2014, prior to melt onset, when the firn aquifer is assumed to be at the seasonal minimum capacity.

To complement surface-based measurements, we use airborne radar data collected by NASA OIB campaign each year between April–May 2010 and April–May 2014. OIB data set is spatially extensive and covers land ice over the ice sheet with an average of 60,000 km of airborne data collected yearly (flight line statistics given in Table 1). On board the NASA OIB airplane, we primarily use the accumulation radar data at a similar frequency range to our ground radar observations. This large airborne radar data set allows us to complement and extend our field observations and provide an ice sheet wide estimate of the firn-aquifer extent and investigate temporal changes in the water table elevation over repeated flight lines.

4. Data

4.1. Airborne Data

Two different radar systems designed and operated by the Center for Remote Sensing of Ice Sheets (CReSIS) on board a NASA OIB aircraft were used in this study [*Rodriguez-Morales et al*., 2013; *Leuschen et al*., 2014a, 2014b]. To monitor extent and depth to the water table (section 5), ultrahigh frequency radar, referred to as the accumulation radar (AR), is used, which operated at a center frequency of 750 MHz and had a bandwidth of 300 MHz. The ultrawide bandwidth enables imaging of internal features, including the water table, with a 65 cm vertical resolution [*Rodriguez-Morales et al*., 2013]. In the along-track dimension, the radar-trace spacing is 35.8 m for a platform velocity of 140 m s^{-1}. For smooth, quasi-specular targets (i.e., internal layers), the imaged area is equal to the first Fresnel zone, which is 20 m at 750 MHz and 500 m height [*Leuschen et al*., 2014a].

In addition to the firn-aquifer water table being identified by AR, the Multichannel Coherent Radar Depth Sounder (MCoRDS), which operates at 195 MHz during the OIB campaigns, is also used to infer aquifer presence [*Leuschen et al*., 2014b].

Finally, we retrieve the along-track surface elevation profile using the NASA Airborne Topographic Mapper (ATM) lidar [*Krabill*, 2013], on board the OIB airplane with the CReSIS radars. The accuracy of the measured elevation is 8.5 cm [*Krabill et al*., 2002]. At nadir, the elevation profile is interpolated to meet the time stamp of each individual traces from the radar data.

4.2. Ground-Based Data

Ground-based radar measurements were made using a 400 MHz ground-penetrating radar (GPR) from Geophysical Survey Systems Inc. The vertical resolution of this system is about ~35 cm for dry firn in West Antarctica [*Spikes et al*., 2004]. We collected 2048 samples per trace in a 500 ns window, for an ~0.24 ns sample interval. Two different types of surveys were performed: one using a snowmobile (2011), moving at ~3 m s^{-1}, and the other using skis (2013 and 2014), moving between 1 and 2 m s^{-1}. Average trace spacing was 0.5 m for the snowmobile surveys and 0.3 m for the ski surveys. Time-dependent gain was used to compensate for radar wave attenuation within the firn. In postprocessing, additional stacking (8 times) increased the signal-to-noise ratio, bringing the average trace spacing to 4.0 m (snowmobile) and 2.4 m (ski).

GPR data are geolocated using a dual-frequency Trimble© R7 GPS receiver in kinematic mode with a sampling interval of ~15 m using snowmobile and ~7.5 m while traveling by skis. We processed the GPS data

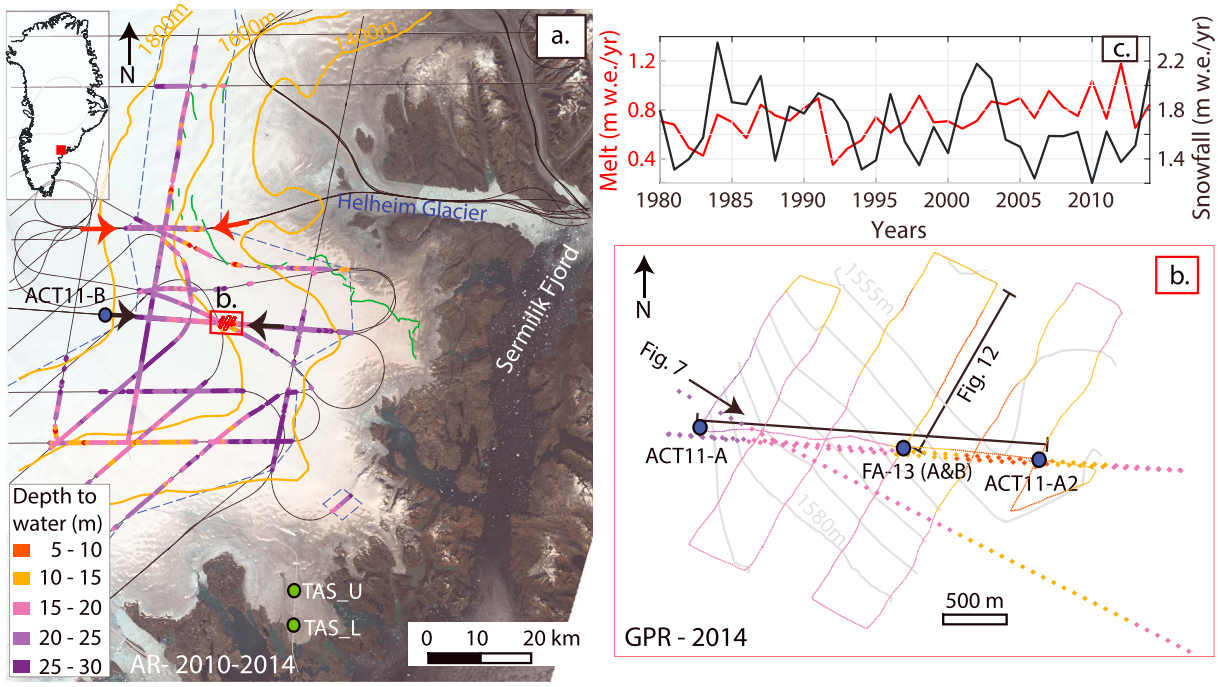

Figure 1. (a) The inset shows a Landsat 8 true color image mosaic (21 August 2014) over the study region. Firn-aquifer locations are color coded by depth to the water table. OIB flight lines are in black. Firn core locations are represented by blue dots, with a two-digit number corresponding to year of collection. The blue dashed line corresponds to the polygon generated from the aquifer linear detections. PROMICE weather stations (TAS_U and TAS_L) are represented with green dots. The green lines indicate the last upstream crevasse visible from L-band SAR imagery [*Moon and Joughin*, 2008]. Elevation contours (orange) are from the 1 km resolution Cryosat-2 DEM [*Helm et al.*, 2014]. (b) The inset details inside the red box with diamonds for airborne depth to water table and lines for the 2014 GPR. The gray elevation contours are obtained from linear interpolation of the GPS grid. (c) The inset shows both the simulated melt (red) and snowfall (black) outputs from the MAR regional climate model (version 3.5.2; at 5 km resolution) at the FA-13 firn-core location [*Fettweis et al.*, 2013].

in 2014 using the precise point positioning web-based processor hosted by the Canadian Spatial Reference Service (CSRS) at https://webapp.geod.nrcan.gc.ca/geod/tools-outils/ppp.php. Formal errors generated by CSRS are averaged for the three field seasons and are estimated at 3.5 cm for latitude and longitude and 7.0 cm for elevation (Figure S1 in the supporting information).

Five density profiles were obtained from our firn cores between 2010 and 2013. Each core section was weighed to retrieve a depth-density profile. The vertical resolution of density measurements was ~1 m in 2010 and 2011 [*Miège et al.*, 2013] and ~20 cm in 2013 [*Koenig et al.*, 2014]. Seasonal snow depth (snow/firn transition) is estimated from the extracted cores, where small ($<$0.8 mm) dry-snow grains transition to larger ($>$1.5 mm) grains with rounded angles, showing evidence of previous melting (Figure S2).

Finally, we use temperature, ablation, and snowfall measurements collected from two Southeast Greenland automatic weather stations (AWSs) in the Programme for Monitoring of the Greenland Ice Sheet (PROMICE) network [*Ahlstrøm and the PROMICE project team*, 2008, www.promice.org]. TAS_L station (65.64°N, 38.90°W; ~270 m above sea level (asl)) and TAS_U station (65.70°N, 38.87°W; ~570 m asl) are located in the ablation area of the ice sheet, with TAS_U being 55 km south of our field site (Figure 1a).

Table 1. AR OIB Flight Campaign Characteristics for 2010–2014 Over Aquifer Regions

OIB Flight Campaign	Total Flight Lines over Greenland Land Ice (km)	Total Linear Distance with Aquifer (km)	Aquifer-Repeat Tracks (km) 2010|2011|2012|2013|2014
2010	30,580	750	+270|210|50|130
2011	74,900	1,040	270 + 345|80|145
2012	86,220	1,130	210|345 + 85|245
2013	42,290	350	50|80|85 + 30
2014	69,790	660	130|145|245|30+
Total	303,780	3,930	660|840|885|245|550

5. Methods

5.1. Radar-Derived Depths to Water

The presence of water in the firn slows electromagnetic wave propagation as it increases the medium's dielectric constant [*Smith and Evans*, 1972]. For soaked-firn conditions, *Smith and Evans* [1972] calculated a dielectric constant of $\varepsilon_f' = 15.2$, about 6 times higher than dry firn ($\varepsilon_f' = 2.4$) with a density of 650 kg m^{-3}. For AR and GPR data, this dielectric contrast produces an interface with high-reflectivity and high-amplitude return, substantially brighter than the dielectric contrast due to dry density changes in the firn column only (see section 6.1 and Figure 3 for details). For the airborne radar, the snow surface was identified and picked using an amplitude threshold at the start of the surface return. This threshold had to be adjusted for each OIB campaign, but no other changes were made in data processing.

The depth to the aquifer surface (water table) is estimated from the two-way travel time (TWTT) of the electromagnetic wave between the snow surface and the water table surface. For nonmagnetic and low-loss dielectric media like snow and firn, the velocity (v) of an electromagnetic wave can be approximated by

$$v = c/\sqrt{\varepsilon'}, \tag{1}$$

where $c = \sim 0.3$ m ns^{-1} is the electromagnetic velocity in a vacuum and ε' is the dielectric permittivity.

We estimate the variations of the dielectric permittivity at depth (above the aquifer) using an empirical relationship linking it to the snow and firn density (ρ) [*Kovacs et al*., 1995]:

$$\varepsilon' = (1 + 0.845\rho(z))^2. \tag{2}$$

A regional steady state ensemble density profile is compiled from five dry firn cores, extracted either above the water table surface or less than 20 km upstream of the firn aquifer. By using an average density profile, we attempt to minimize the impact of small-scale spatial density heterogeneities in the firn of the lower percolation zone. We also use a biexponential fit to smooth and interpolate the averaged density profile with depth.

The presence of water within the snow microstructure influences the TWTT to depth conversion within the firn aquifer, since water slows the transmitted electromagnetic waves [e.g., *Bradford et al*., 2009]. Here in focusing on the water table depth, we assume that firn above the water table is dry when measurements are made in the spring (April–May), consistent firn temperature profiles collected at our field site [*Koenig et al*., 2014].

5.2. Associated Uncertainties

There are two main uncertainties in mapping the spatial extent of the firn aquifer and its depth to the water table with AR radar: (1) the uncertainty linked to the presence or absence of the firn aquifer and (2) the uncertainty in determining the depth to the water table, if present. Picking of the water table was not a fully automated process, and thus, a subjective human bias is introduced. We did not use a constant brightness threshold to detect the water table from the radar data as brightness levels varied substantially based on the radar system used (GPR versus AR), the year of collection of the AR radar, the depth to the reflector, and the location. A length of ~60,000 km of radar profiles was flown over the Greenland ice sheet during each OIB campaign (2010–2014; Table 1). For each flight line, we manually examine radar data for bright and continuous reflectors, at a depth range of 5–50 m [*Forster et al*., 2014]. We identify a water table by the presence of continuous reflector that can be followed for more than 0.5 km along profile. To quantify the human bias introduced from the layer picking, the entire 2011 OIB data set was processed by two different operators, using two different tracing methods: manual and semiautomatic. The semiautomatic routine is based on an edge-detection method, looking at differences between lower and upper frequencies to accentuate the peaks. The automatic part of the picker performed well in regions with clear water table signal, but manual tracing was required for weaker signals. We find agreement (within uncertainties) over 75% of the total area between the two operators. This difference between picks is structured and mainly occurred in locations where internal reflectors were weak in the radar data. Discrepancies between layer picks occur on the edges of the water table, where reflector intensity diminishes gradually.

Radar data quality and aquifer detections depend on airplane survey conditions, such as turbulence and turning geometry. For example, aircraft roll greater than 10° prevents detection of internal layers and, as a

result, identification of the firn aquifer. Identifying deeper water tables is challenging due to the greater attenuation of the higher-frequency radar wave of the AR. Usually, an aquifer deeper than 40 m in the percolation zone is not well imaged in the AR profile, likely due to weak returns from internal layers that are masked by surface clutter (off-vertical surface) at the edges of the percolation zone.

Layer depth uncertainty comes from two sources: TWTT-to-depth conversion (section 5.1) and layer picking. The TWTT-to-depth conversion uncertainty is associated with the density profile used. For example, within $\pm 1\sigma$ (standard deviation of the averaged density) of density, the uncertainty is ± 40 cm for an average depth to the water table of 20 m. For the 2011 AR data, the layer picking was repeated twice, using a semiautomatic approach and a manual approach. The averaged depth difference was 60 cm for the ~1000 km of radar data (~50,000 radar traces). Internal reflecting horizons imaged by the GPR were brighter and more distinct than those imaged by the AR, probably due to the lack of surface clutter that obscured the deeper returns in the AR. The repeated picking test over a 5 km segment shows an averaged difference of only 7 cm (or three samples) between the two picking methods. Finally, we calculate averaged error propagations based on the two uncorrelated uncertainties of 72 cm for the AR and 41 cm for the GPR, which remain small compared to the range of water table depths investigated (4–40 m; see Figure 6).

5.3. Estimation of Firn-Aquifer Extent

We use five consecutive years of AR radar data (2010–2014) to estimate the spatial extent of firn aquifers. For this analysis, we assume that the extent of firn aquifers is in steady state over the 5 year period to allow interpolation of aquifer extent between OIB flight lines. To convert the linear distance (km) obtained by radar profiling to an area estimate (km^2), we invoke constraints along the across-flight line direction and consider four cases (Figure 2). Cases (a) and (b) are "isolated-aquifer detections" in which there is only one flight line and no crossover points. For aquifer detections over linear distances less than 5 km (case (a)), we use the along-flight line aquifer length to estimate the aquifer dimension in the across-track direction, creating a squared area. For linear distances greater than 5 km (case (b)), we limit the aquifer dimension in the across-flight line direction to 5 km creating a rectangle around the flight line. We use a 5 km threshold based on examination of the connected-aquifer detection, but the choice remains somewhat arbitrary. Case (c) is characterized by multiple flight lines with one more crossover points; here we use the end points of the profiles delineating the aquifer to define a polygon (Figure 2). Case (d) is characterized by the two parallel flight tracks closer than 10 km with a detected aquifer. We assume that the area between the two flight lines also contains water and connect them into a polygon. The two parallel flight lines cannot be separated by more than 10 km; otherwise, they would be included in case (a) or (b). Finally, we allow in a given polygon linear gaps less than 10 km, gaps which may potentially be due to aquifer detection deficiencies during radar data collection, often linked to plane geometry, e.g., airplane roll greater than 10°.

5.4. The 2-D Lateral Flow Model

We use SEEP2D, a 2-D finite element groundwater flow model within the Groundwater Modeling System package [*Jones*, 1999], to help explain lateral changes in the aquifer extent in the upper part of Helheim Glacier. We combine radar data with laser altimetry to obtain a continuous measurement of the water table elevation relative to the surface topography along an ice-flow line. We assign a head value to each node along the water table as a boundary condition. The head value corresponds to the water surface elevation inferred from the radar (one radar trace every 16 m in average). A uniform hydraulic conductivity range between 1×10^{-5} and 5×10^{-5} m s^{-1} is used throughout the aquifer [*Fountain and Walder*, 1998] to deduce volumetric flow rate, and we assume a constant aquifer thickness of 25 m [*Koenig et al.*, 2014]. To summarize, three assumptions are made: (1) unconfined firn aquifer at steady state, (2) constant aquifer thickness, and (3) a constant hydraulic conductivity value taken from mountain glacier observations. This modeling approach uses only water table and surface elevations to simulate an aquifer flow pattern at steady state without accounting for seasonal meltwater input. For future work, adding meteorological forcing, thermodynamics, crevasses, and third dimension to this model will be essential to better constrain and simulate firn-aquifer seasonal recharge, local discharge, refreezing, lateral flow, and drainage, but this remains beyond the scope of this study.

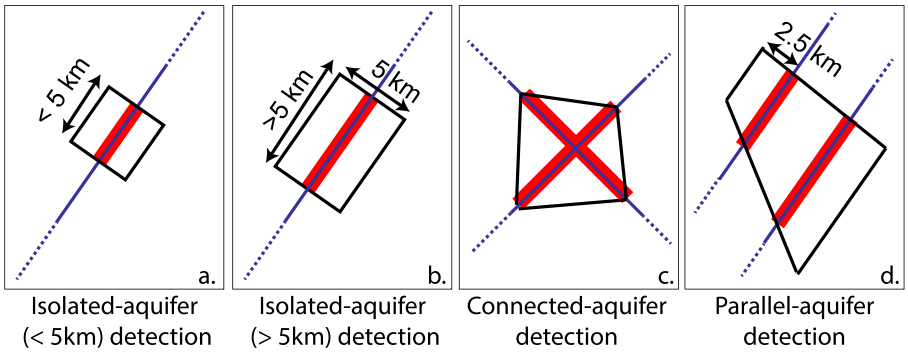

Figure 2. (a–d) Schematic of the four different aquifer detection cases used to delineate polygons and convert linear aquifer distance derived from radar observations into aquifer area. Flight lines are in blue, firn-aquifer detections in red, and the deduced area in black. For aquifer detections over 5 km, a set 5 km distance perpendicular to the flight line is used as threshold to create polygons.

6. Results

6.1. Firn-Aquifer Identification

The last meter-long segments of firn cores ACT11-A (1 May 2011) and ACT11-A2 (30 April 2011) were retrieved in water-saturated firn at 25.3 ± 0.5 m and at 10.4 ± 0.5 m depth, respectively (Figure 1 for core location). Within an 11 day time interval, AR and GPR data imaged a bright reflector at similar depths (Figure 3) [*Forster et al.*, 2014]. The high correlation coefficient ($r = 0.995$) between the water table depth observations from the two radars gives us confidence in our ability to map the firn aquifer with only AR [*Forster et al.*, 2014].

The AR and MCoRDS systems have operated simultaneously onboard the NASA P-3 aircraft since 2010, allowing for a direct comparison of the two systems in aquifer regions (Figure 4, for a profile located between red arrows in Figure 1). There is good agreement found between the presence of weak, intermittent, or missing bed echoes in the MCoRDS data and the presence of a water-saturated firn layer as detected by the AR (Figure 4). From the MCoRDS data only we can infer the presence or absence of water in the firn layer,

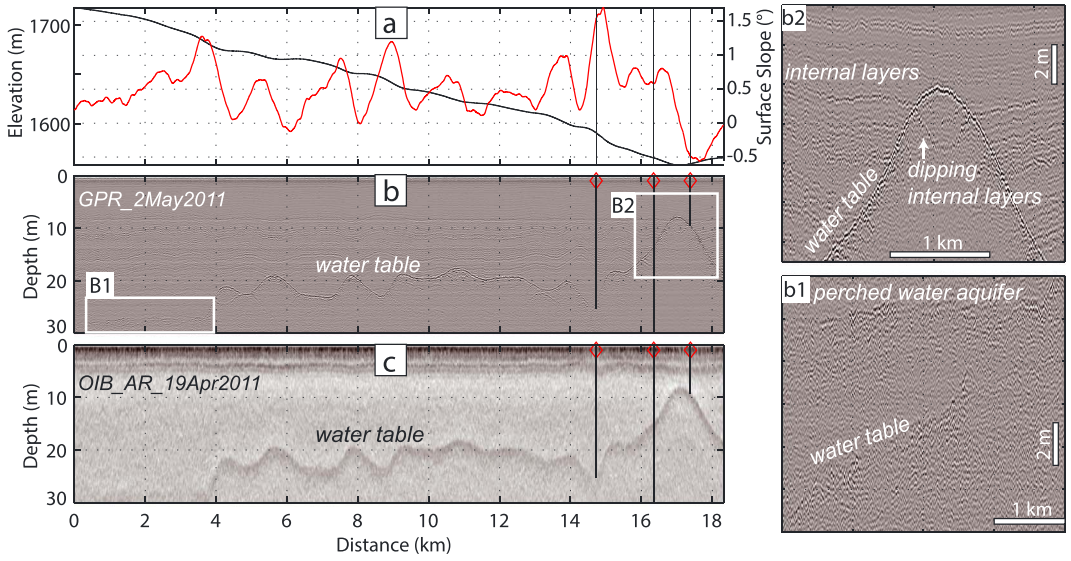

Figure 3. (a) The inset represents the surface elevation (black) and surface slope (red) both retrieved from OIB ATM data [*Krabill*, 2013]. Direct comparison (correlation coefficient of $r = 0.995$) between (b) GPR (400 MHz; 2 May 2011) and (c) AR (750 MHz; 19 April 2011) over an 18 km portion of the ACT-11 traverse (transect is located between the two black arrows on the map of Figure 1). The three boreholes (black diamonds and vertical lines) confirm the presence of water at the bright reflector depth. The insets in Figures 3b1 and 3b2 show the details of the GPR data.

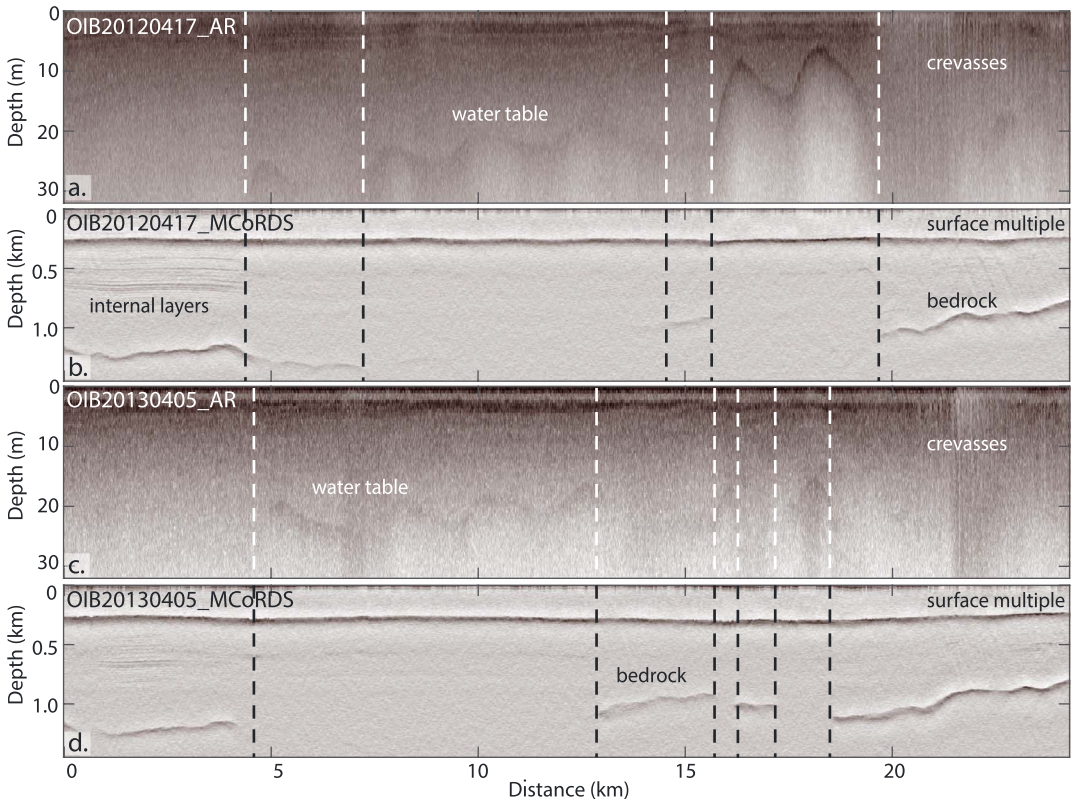

Figure 4. (a and c) Accumulation radar at 750 MHz and (b and d) MCoRDS at 195 MHz profiles over the firn aquifer in the upper part of Helheim Glacier collected on 17 April 2012 and 5 April 2013. Missing bed reflections in the MCoRDS radar correlate with the presence of a water-saturated firn layer as illustrated by vertical dashed lines that indicate coincident transitions in both radar profile. Profiles are located between the two red arrows in Figure 1.

although we cannot estimate the depth to the water table. Other causes for missing bed echoes in the MCoRDS cannot be excluded, such as possible changes in the englacial and basal condition, but these other causes seem unlikely, given that the surface return and its multiples do not change in strength substantially across the aquifer transition. In addition, the relative amplitude differences of ice-bottom scattering are negligible without the aquifer between two points, as the relative ice-bottom scattering between the same points is large when the aquifer is present at one point. Finally, internal layers disappear simultaneously with the loss of the bed reflection, suggesting that the latter cannot be related to changes in basal conditions alone (Figure 4).

6.2. Firn-Aquifer Extent

We use data from five consecutive OIB seasons (2010–2014) to map the presence of firn aquifers over the Greenland ice sheet. To estimate the total aquifer area, 110 polygons were created with areas ranging from 1 km^2 to 9600 km^2 (Figure 5); polygons less than 1 km^2 were discarded. Roughly half of the firn-aquifer area is found in southeastern Greenland with a total of 10,690 km^2 (Figure 5c). The southern tip of the ice sheet represents the second largest aquifer region (35%) with a total area of 7230 km^2 (Figure 5d). In eastern Greenland, smaller aquifers are detected for a total area of 2200 km^2 (10%), mainly south of Kangerlussuaq Glacier, with a few isolated aquifers on the Geikie Plateau (Figure 5). For western Greenland, the Sukkertoppen ice cap has high accumulation rates and a small aquifer (150 km^2) persists for at least the 4 years of our study (2010–2014). In a lower and narrower elevation band (1070 $\pm$ 150 m), a few isolated aquifers (5%) are found in northwestern Greenland (total area of 1230 km^2). No aquifers were identified in the northeast portion of the ice sheet (Figure 5).

With a mean elevation at 1615 $\pm$ 300 m and a mean accumulation rate of 1.0 $\pm$ 0.4 m w.e. yr^{-1}, most of the firn aquifers are found below the 2000 m contour line, except for the southern tip of the ice sheet where

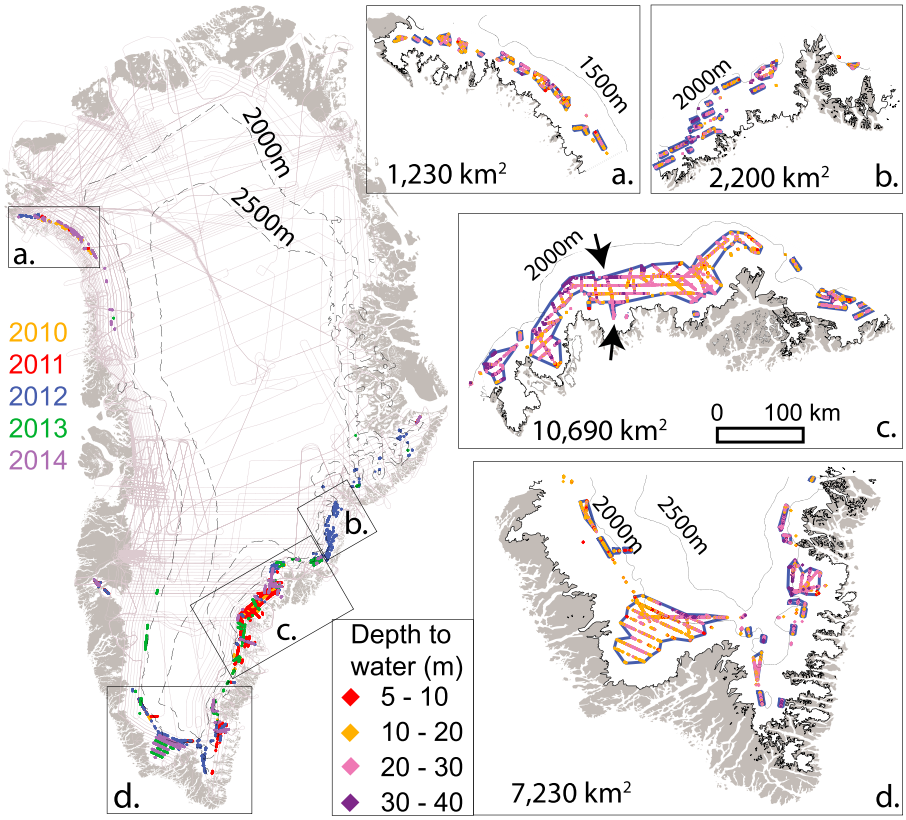

Figure 5. The ice sheet wide map shows the firn aquifers mapped from AR data for 2010–2014 (colored by detection year). OIB flight lines are in light gray. (a–d) The four different insets present the depth to the water table for the 5 year combined data set. The two black arrows (Figure 5c) show the AR profile location of Figure 10. The polygons contoured in blue are used to estimate aquifer extents for each inset. Figures 3b and 3c have a 40° angle from geographic north. All inset maps are at the same spatial scale. Coastline, ice mask, and 1 km DEM are from *Rignot and Mouginot* [2012], *Howat et al.* [2014], and *Helm et al.* [2014], respectively.

aquifers extend up to the 2200 m contour (Figures 5 and 6). A total linear distance of 3930 km of firn aquifers were imaged in the five spring airborne surveys (Table 1), yielding a total estimated area of 21,900 km^2. Due to the varying nature of OIB flight lines, sampling bias always exists and surface elevations are not equally sampled across flight campaigns (Figure 6a). The depth to the water table is normal distributed over the 5 year survey period with a mean of 22 ± 7 m, implying a minor bias for this time period (Figure 6b). The mean accumulation in aquifer regions ranges between 0.4 and 1.6 m w.e. yr^{-1}, based on a Calibrated Polar MM5 simulation [*Burgess et al.*, 2010] (Figure 6c). The total radar-derived firn-aquifer area is about 3.5 times less than the Regional Atmospheric Climate Model (RACMO2) simulation (70,000 km^2) of the water-saturated firn layer for April 2011 [*Forster et al.*, 2014]. To explain this discrepancy, we suggest that the radar-derived aquifer extent is a lower bound estimate, as it is biased by flight line locations and the need for sufficient water to be detected in the radar data. In contrast, the RACMO2 liquid-water-content estimate is more likely to represent an upper bound estimate for aquifer total area. RACMO2 simulates water overwintering in firn for locations where no aquifers are detected in the AR, but this may be due to the fact that the RACMO2 aquifer-extent estimate includes relatively small water amounts ($<$200 kg m^{-2}) integrated over the entire firn column thickness [*Forster et al.*, 2014]. This could likely be below the detection limits of the AR since no water table might be present but only small amount of water held by capillary forces.

6.3. Temporal Evolution

Radar measurements repeated over the same locations allow the interannual monitoring of firn-aquifer variations (Figure 1). Two transects are selected, one located at our Ridgeline field site with ground-based radar profiles and the other on a Helheim Glacier ice-flow line, where airborne radar repeat profiles exist in close

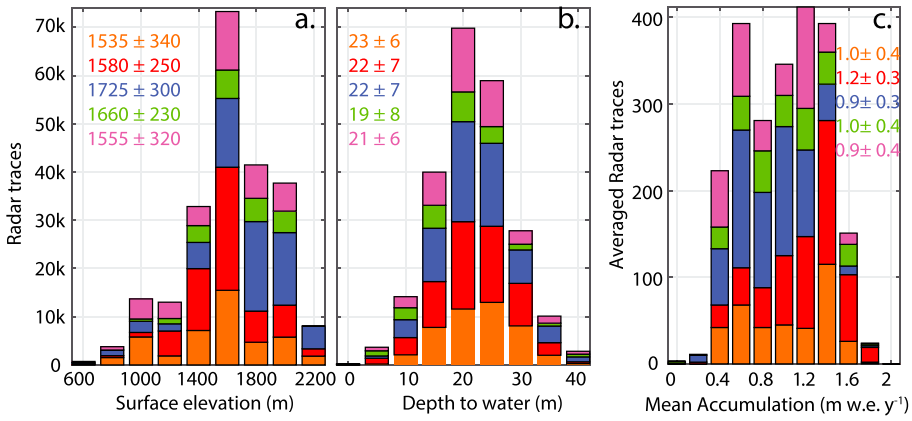

Figure 6. Firn-aquifer (a) surface-elevation, (b) depth-to-water, and (c) mean-accumulation rate distributions for 5 years of airborne radar data: 2010 (orange), 2011 (red), 2012 (blue), 2013 (green), and 2014 (magenta). Mean and ±1 standard deviation are given for each year. The mean accumulation rate is simulated by Calibrated Polar MM5 between 1958 and 2007 [*Burgess et al.*, 2010].

proximity to our Ridgeline Site (~20 km). Since the radar tracks are not exactly superposed between years (up to 220 m of horizontal differences for AR), we linearly interpolate the radar data to a given profile to avoid image distortions.

At our Ridgeline Site, a GPR profile (~2.5 km) was first collected in May 2011 and then resurveyed in April 2013 and April 2014 between two firn-core locations (ACT11-A and ACT11-A2; Figures 1 and 7). In 2012, the same transect was overflown by OIB allowing us to fill the temporal gap with AR data. We record temporal changes of the water table elevation as the difference between the snow surface elevation and the depth to the water table between two consecutive years (Figure 7b). Along this transect the average snow surface lowered by 0.4, 1.4, and 1.0 m for 2011–2012, 2012–2013, and 2013–2014, respectively. The water table elevation does not follow the same trend. After a 0.6 m average lowering between 2011 and 2012, the water table rose by 1.1 m in 2013, illustrating filling from the more extensive melt year of 2012. Later, in 2014, the mean water table is 2.5 m deeper than in 2013. To put this lowering in context, we look at possible differences in the amount of seasonal snow but find that seasonal snow depth was about 280 cm on 6 April 2013 and 300 cm on 10 April 2014, rather similar. In addition, we compare the vertical stratigraphy from four firn cores extracted above the water table to observe changes in ice lenses to firn ratio over time (Table 2 and Figure 1

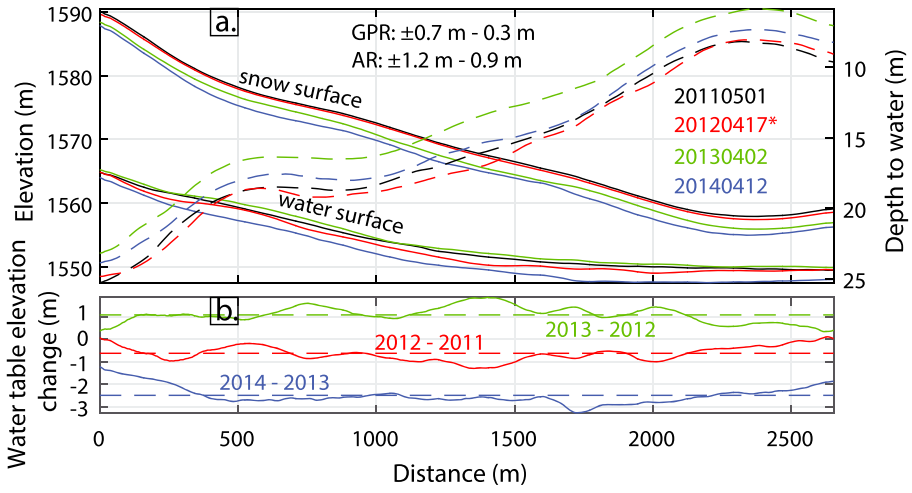

Figure 7. Temporal evolution of the snow surface and the water table depth from GPR data for 2011, 2013, and 2014 and from AR data for 2012*, along profile between two firn-core sites (ACT11-A to ACT11-A2; Figure 1). (a) The snow-surface elevations, water-surface elevations (solid lines), and the water table depths (dashed lines) for the 4 years. (b) The water table elevation changes between two consecutive years. The uncertainty bounds (Figure 7a) are estimated at both ends of the profile.

Table 2. Depth to Water and Ice Fraction of the Different Firn Cores Collected During Fieldwork (Figure 1)[a]

Firn Cores	Elevation (m)	Depth to Water (m)	Ice Fraction (%)
ACT11-A	1589	25	14
ACT11-A2	1559	10	7
FA13-A	1563	12.2	9
FA13-B	1563	12.2	8

[a]The two-digit numbers in the firn-core names give the year of collection. Note that FA13-A and B are only located 2 m apart.

for core locations). From the snow surface to the water table, ice lenses represent less than 10% of the dry firn column, and no obvious increase is observed over the short 2 year period, even though it included the stronger 2012 melt year (Table 2). We hypothesize that the water table lowering observed in 2014 is due to a combination of a decrease in surface meltwater production while lateral water flow and drainage remained more or less constant.

The second study transect is located in the upper part of Helheim Glacier between 2010 and 2014 (Figures 4 and 8). The first measurement in spring 2010 was made shortly before the above-average 2010 summer melt [*Fettweis et al.*, 2013] (Figure 1c) that produced an average rise of 1.8 ± 0.9 m in the water table elevation by spring 2011. The water table elevation lowered by 1.0 ± 0.6 m between 2011 and 2012, and a 3 km upstream extension of the aquifer is observed in 2012. At the lower elevation end, the water table undulates, following the surface topography, before encountering crevasses, where the bright return from the top of the water table disappears (~19 km in Figure 4a). In 2013, consistent with MCoRDS observations, the water table is substantially lowered or missing between 13 and 18 km (Figures 4c and 4d). In contrast, on the upper end of the profile (5 to 12 km), the water table elevation increased by 3.3 ± 0.4 m between 2012 and 2013 and finally lowered by 0.8 ± 0.8 m between 2013 and 2014. All the water table elevation changes between 2010 and 2014 are compiled in Figure 8. In addition, from the ATM elevation data collected over the 12 km long transect simultaneously with the AR, we observe an average 1.0 ± 0.4 m surface lowering between the springs of 2011 and 2012, and a 1.5 ± 0.5 m surface lowering between springs 2010–2011 and 2012–2013, in agreement with the two above-average summer melt years of 2010 and 2012. For those two years, large meltwater production increased meltwater percolation and therefore increased recharge of the firn aquifer.

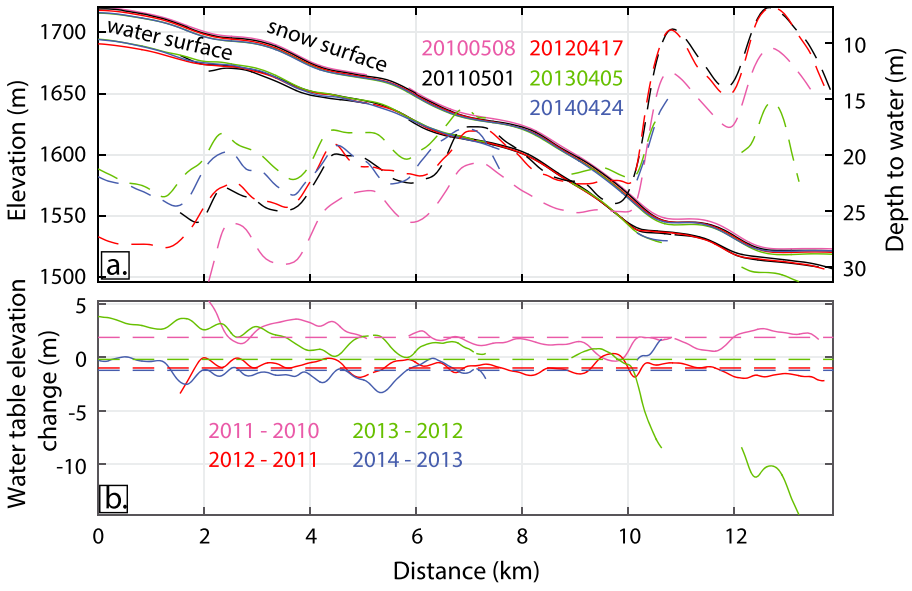

Figure 8. Temporal evolution of the snow surface and the water table depth from AR data for 2010–2014 for the upper Helheim Glacier (between red arrows in Figure 1). (a) The snow-surface elevations, water-surface elevations (solid lines), and water table depths (dashed lines) for the 5 years. (b) The water table elevation changes between two consecutive years.

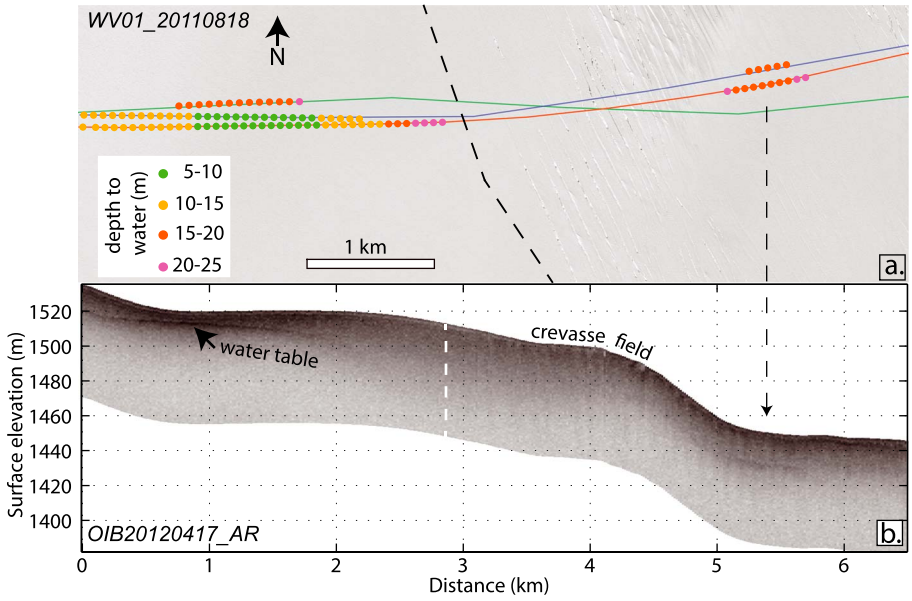

Figure 9. Lower end of the firn aquifer in relation to crevasses for the upper part of Helheim Glacier (starts at 11 km in Figure 8). (a) The WorldView01 image from ©DigitalGlobe with a 0.5 m resolution. The colors indicate the depths to the water table in meters. The flight lines in red, blue, and green represent the OIB data from 2011, 2012, and 2013, respectively. The dashed line indicates the last upstream crevasse visible in close proximity to the firn-aquifer edge.

6.4. Lateral Boundaries

The lateral limits of the Ridgeline Site aquifer are studied for the two transects using the GPR (upper elevation limit) and AR (lower elevation limit) data. The AR can cover crevassed terrain, whereas the GPR provides greater penetration depth and finer detail at the upper end of the firn aquifer. We find that the upper elevation transition (~1700 m along the ACT traverse) between dry and wet firn is gradual and diffuse. In Figure 3 b1, two brighter reflectors are found in the GPR profile at depths between 30 and 40 m but with some short discontinuities. This suggests that the upglacier firn-aquifer expansion is sensitive to surface meltwater input and surface topography. Also, we note that these two brighter reflectors observed in the GPR data are not well defined in the AR data (Figure 3); we postulate that the AR might be less sensitive to small amounts of water ($<$200 kg m^{-2}), particularly at greater depths ($>$30 m). The low-elevation end of the aquifer is investigated using AR data, coupled with ~0.5 m resolution visible satellite imagery (WorldView-1, DigitalGlobe©). The upper crevasses are imaged by the AR, as vertical stripes locally disrupting the internal layers (Figure 9). Combining the AR profile with the satellite images, we note that the lower elevation edge of the water table is a sharp boundary and corresponds to the initial encounter of the crevassed area, implying that water drains into them. The exact depths of the crevasses are unknown; however, due to the loss of the aquifer reflector, it can be assumed that they at least reached the water table. Our current measurements do not allow us to investigate the fate of the water once it reaches the crevasses, but it is likely that some water enters the englacial network, possibly reaching the bedrock. In Figure 9, the upper crevasses (4–5 km) are located on a steep section, and a bright reflector is observed lower down, where the slope decreases and there no visible crevasses nearby (5–6 km). The relationship between firn aquifers, crevasses, and the impact of water flow are further addressed in section 7.

6.5. Unconfined Firn Aquifer

Radar imagery shows stacked sequences of internal reflection horizons in the dry firn above the water table, layers that represent density contrasts from the accumulation and melt histories. Throughout the study area we find places where these internal reflection horizons intersect the water table at an angle (Figure 3b2). After showing that the water table fluctuates in the radar data from year to year, the fact that the water table intersects preexisting internal layering implies that lateral flow of water is influenced by the surface slope and not bounded by possible laterally extensive refrozen ice layers. This observation, coupled with the interannual repeat radar profiles, shows the free vertical bound of the water table and gives an unconfined behavior

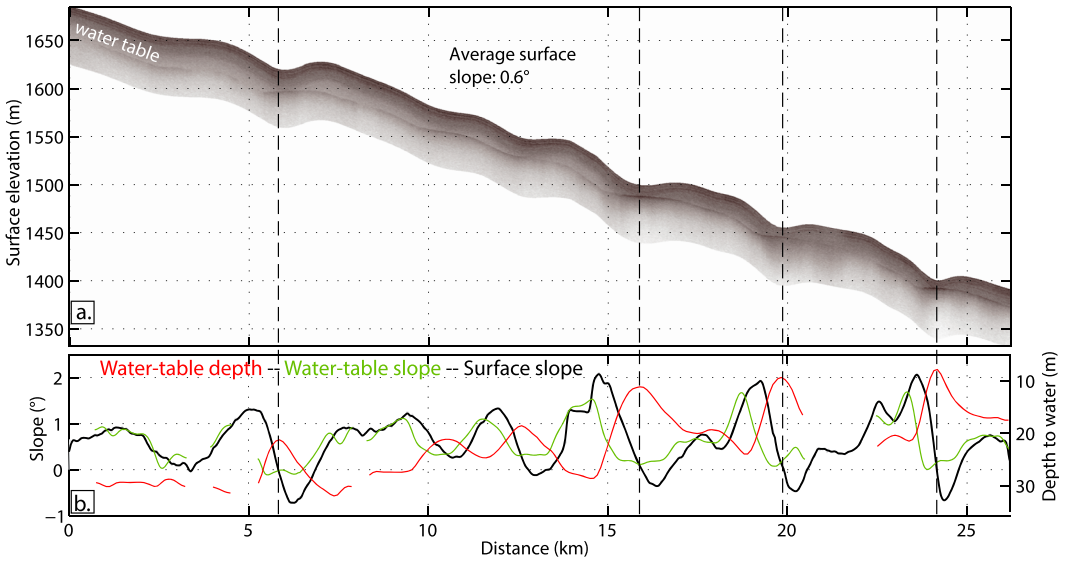

Figure 10. (a) AR profile (2011) corrected for topography using the ATM elevation data [*Krabill*, 2013]. Profile location is shown in Figure 5c and is oriented perpendicular to elevation contours. (b) The inset corresponds to the water table depth (red), the surface slope (black), and water table slope (green). The vertical dashed lines illustrate that local minimum water table depths are observed when the surface slope intersects 0.

to the aquifer. This is consistent with the unconfined firn aquifers observed on other glaciers [*Fountain and Walder*, 1998; *Christianson et al*., 2015]. The thickness of the unconfined aquifer is unknown; at the GPR and AR frequencies the bottom of the aquifer, where water-saturated firn transitions to glacial ice, is not detected.

The unconfined aquifer assumption allows continuous hydraulic head estimates to be made directly from the depth of the water table along the radar profile. Figure 10 illustrates the water table imaged by the AR over a 25 km along-flow transect, corrected for topography. Small-scale surface undulations (<5 km) with, for example, 50 m of elevation changes are associated with water table fluctuations up to 20 m (Figure 10). Over the full length of the profile (~25 km), the water table is deeper in the upper part, with a gradual decrease in the depth to the water table; consistent with those made on mountain glacier aquifers, although the latter have shorter aquifer lateral extents [*Fountain*, 1989]. Along our profile, the average surface slope is 0.64° and the averaged hydraulic gradient is 0.01 (water table slope of 0.61°), 10 times lower than at Storglaciären (0.1 for a water table slope of 7.1°) [*Schneider*, 1999]. Minima in the depth to the water table coincide with areas where the surface slope is flat; this is found extensively in our airborne data as well as along other radar transects.

6.6. The 2-D Simulated Flow

SEEP2D simulates the flow of water within the firn aquifer while using the variables, assumptions, and boundary conditions described in section 5.4. Figure 11 shows the simulated local flow cells [*Tóth*, 1963]; their size depends on surface undulations, and the spacing between flow lines decreases with increasing water velocity. To interpret the groundwater simulation, we assume that Darcy's law is valid and that there is no flow into or out of the plane of the cross section (i.e., 2-D flow). Following Darcy's law, the volumetric flow rate Q ($m^3\,s^{-1}$) of an incompressible fluid is calculated under stationary conditions within a porous medium of the cross-sectional profile area A (m^2), and length ΔL (m) under a head difference ΔH (m), which represents the hydraulic gradient [*Schneider*, 1999]. These three variables (A, L, and H) are taken from the AR profile from spring 2012 over an ~12 km long section (Figure 11).

$$Q = K\ A\frac{\Delta H}{\Delta L} \tag{3}$$

We obtain an averaged total flow rate (Q) ranging between 3300 and 16,500 $m^3\,yr^{-1}$ per meter width of the profile, based on a hydraulic conductivity (K) range between 1×10^{-5} and $5\times10^{-5}\,m\,s^{-1}$, taken from

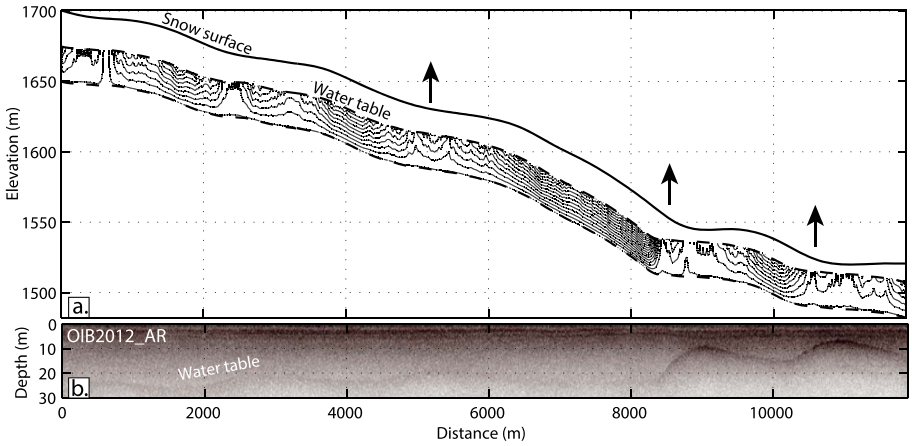

Figure 11. (a) The steady state flow lines (solid) simulated using 2-D flow model using water table and an assumed aquifer thickness (25 m) as boundary conditions (dashed). The vertical arrows represent the local discharge locations that occur at steep/flat transitions. (b) The AR profile used to retrieve the depth to water (similar to profile of Figure 4a, located between red arrows in Figure 1).

mountain glacier studies [*Fountain and Walder*, 1998]. The flow rate needs to be taken with caution, as it is directly proportional to the assumed value of *K*, which has not been measured directly at our field site. Fluctuations in head translate to variations in drainage rates; as such, the drainage rate is not constant throughout the aquifer. Spatial undulations of the water table can imply that local flow cells are created in the aquifer with a similar scale to undulations of the surface topography (typically less than 10 km). The local flow cells are strongly related to the local topography (Figure 11). Local surface depressions (vertical arrows in Figure 11) may act as local discharge locations of the firn aquifer, as is discussed in section 7.2.

7. Discussion

7.1. Firn-Aquifer Variability

We study the temporal and spatial variabilities of the firn aquifer on AR profiles in the upper part of Helheim and at our field location (Ridgeline site), where repeated data are available. At the field location, the firn-aquifer lateral extent appears stable between the springs of 2011 and 2012, but both snow-surface elevation and water table elevation decreased (Figure 7). The relatively constant depth to the water table between these 2 years implies that water discharge was able to accommodate additional meltwater input, if any. The vertical rise (+1.1 m) of the water table observed in spring 2013 is likely due to a combination of an increase in surface melt in summer 2012, compared to 2011, and a reduction in snowfall prior to data collection. Data from nearby AWSs confirm that accumulated snowfall was 40% less in 2013, compared to the 2008–2014 mean, and that the annual mass loss in 2011 was ~5% below average, whereas 2012 was ~20% above average. However, the rise of the water table observed in 2013 may not simply represent an increase in water volume storage. For the Storglaciären firn aquifer, *Schneider* [1999] observed that the rise of the water table was similar to the rise of firn/ice transition (~1.5 m yr^{-1}), meaning that the aquifer thickness was relatively constant. In our study, the lack of radar signal penetration through the aquifer prevents us from evaluating this conclusion. The following winter (2013–2014) corresponded to another low snowfall year (50% less than the 2008–2014 average), from the AWS data, but the aquifer water level dropped (−2.5 m). This lowering can be explained by lateral water flow in the aquifer, associated with lower input of new meltwater, depleting the water from these elevations. In case of shallow water tables, usually located less than10 m from the surface, it is not excluded that refreezing from the winter cold wave might contribute to lowering the water table. From the AWS data, 2013 was a relatively low melt year, with ablation rates 20% below average, implying that less meltwater was produced.

The OIB repeat radar surveys in the upper part of Helheim Glacier present a strong case for partial drainage of the firn aquifer after spring 2012. Between 2012 and 2013, the aquifer disappeared at low elevations, while the water surface rose at higher elevations (Figures 4 and 8). The absence of radar reflectors can be due to (1) water drainage, (2) refreezing, or (3) reduced penetration of the AR signal. We favor the drainage

hypothesis by ruling out the other two possibilities. Refreezing seems unlikely, after the above-average summer melt of 2012; it would be difficult to refreeze substantial amounts of water in the firn, which would have been temperate over a few years, particularly since, based on the AWS temperature data, winter temperatures were not abnormally cold. Reduced penetration of AR radar signal also seems unlikely. We use a continuous bright radar reflector in the AR data to infer the presence of a water table; its absence might be due to thick ice layers preventing the radar signal from reaching greater depths (>10 m). But even if the AR signal (750 MHz) was attenuated, the lower-frequency MCoRDS system (195 MHz) would have been able to indicate water. However, the MCoRDS profile shows clear bed-echo returns over the lower part of the profile (Figure 4). Drainage of a 5 km stretch of the aquifer implies that hydraulic gradients and hydraulic conductivity must be high enough to mobilize a large volume of water and remove it, presumably into crevasses. This lower part of the aquifer appears to be decoupled from the upper part, at least temporarily, until it can be recharged either from seasonal surface meltwater production or from upstream water flowing laterally downglacier. Based on nearby AWS data, summer 2013 melt was below the 2008–2014 average, and the low-elevation end of the aquifer stayed dry in spring 2014.

7.2. Lateral Water Flow

Hydraulic gradient is the main driver of the water flow over the relatively flat surface of the Greenland ice sheet. For mountain glacier aquifers, hydraulic gradients can be up to 10 times greater than the ones for the ice sheet but over smaller lateral extents; the steeper gradients route meltwater more efficiently, thus limiting water from overwintering. The hydraulic gradient is related to the firn-aquifer thickness and surface slope [*Jansson et al.*, 2003]. For our study transect, the hydraulic gradient is 0.01 on average, an order of magnitude lower than Storglaciären [*Schneider*, 1999], implying the presence of thicker firn aquifers within the ice sheet. However, as the hydraulic gradients vary spatially following ice sheet surface undulations, the aquifer thickness is expected to be variable.

In the percolation zone, the presence of ice lenses complicates water percolation. Horizontal ice lenses disrupt the vertical flow of water, forcing it to flow horizontally [*Conway and Benedict*, 1994]. On the Devon Ice Cap and in West Greenland, thick and continuous ice lenses force meltwater to pool above them and flow laterally downstream either to run off or refreeze at the end of the melt season [*Gascon et al.*, 2013; *Machguth et al.*, 2016]. At our field location, during the spring 2014, the GPR profile suggests slow downstream migration of water, following hydraulic gradients (Figure 12). In this figure, the water surface happens to diverge from the water table while the surface slope reaches 0°. A thick ice layer, which creates an impermeable boundary, could have been encountered by the water. The water pools on this horizon and expands laterally, slowly flowing downstream at the firn ice interface, saturating the above firn. This feature is thought to be a perched water-saturated firn layer on top of the firn aquifer. The sharp termination of the reflector on the flatter portion of the radar profile implies that lateral water flow was active, progressing downslope (white arrow in Figure 12). In concordance with low hydraulic gradients, we infer a slow lateral motion of water during the winter, but we did not monitor its

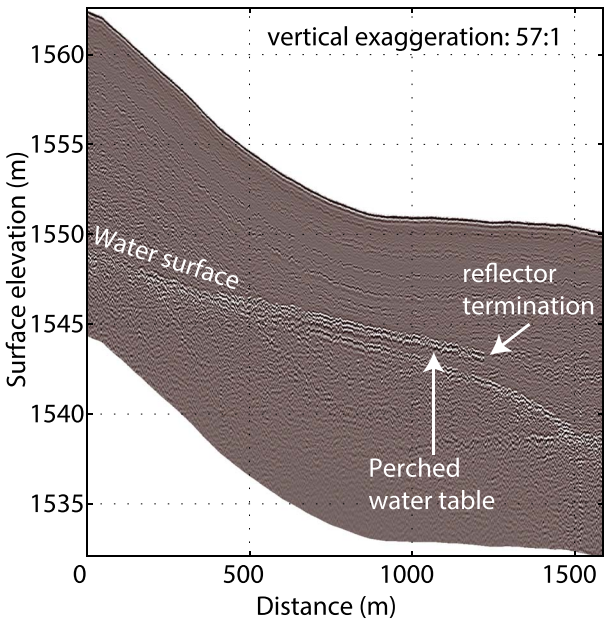

Figure 12. GPR profile from April 2014, corrected for surface elevation, over a 1.5 km segment (Figure 1). A perched water table is observed ~1–2 m above the firn-aquifer surface, interpreted as water ponding on an ice layer and traveling downglacier under low hydraulic gradients.

changes in real time. This observation is consistent with observations from *Humphrey et al*. [2012], showing that deep pore water slowly migrates downglacier under low hydraulic gradients.

Based on our hydraulic simulations, flow cells are revealed and the transition "steep to flat" marks the succession of local water discharge areas within the larger aquifer (~12 km), indicating local flow patterns (2–3 km; Figure 11). This pattern was expected due to the undulating water table inferred from the radar data. These local discharge features are located in surface depressions and seem to be transient, increasing the water level temporally due to additional water coming from a steeper uphill. This process seems to happen throughout the fall and winter (after the melt season shutdown) as the lateral flow evidence observed in Figure 12 for early spring. However, our 2-D simulation does not include 3-D effects in water flow occurring if flight lines do not intersect surface undulations at the lowest point of a given depression. Such a scenario would make water flow in a direction that is not parallel to an ice-flow line, therefore not parallel to our 2-D flow model, moving spatially the simulated discharge locations. If the hydraulic gradients were steep enough, we would have observed water tables intersecting the surface in a few instances elsewhere over the ice sheet in the AR data. Additionally, *Christianson et al*. [2015] reported water near or at the surface in a topographic depression for the Holtedahlfonna firn aquifer in winter, consistent with low backscatter radar signals from satellites. As a result, the near-surface water becomes sensitive to the cold winter temperature and partial to complete refreezing would occur based on the amount of water. In west Greenland, water discharge has also been observed, and *Humphrey et al*. [2012] documented the presence of pingo-type features (usually found in permafrost) forming at similar locations to our local water discharge simulations (Figure 11), where the slope transitions from steep to flat.

7.3. Impacts of Firn Aquifers

The impact of firn aquifers on broader ice sheet mass balance and hydrologic systems must be considered since stored water within the aquifer influences firn densification, the mass of the firn column, and influences meltwater runoff routing and timing. Currently, firn models implemented in regional climate models have a water-retention scheme that only allows water to be held in the firn by capillary forces [e.g., *Kuipers Munneke et al*., 2014]. This model assumption results in underestimation of water storage in firn-aquifer regions, as it neglects the storage term at the firn-ice transition, where water tends to pool. Additionally, drainage from the firn aquifer, such as we observe between 2012 and 2013, can impact ice dynamics by delivering meltwater to the ice sheet bed or by increasing the ice temperature, contributing to cryo-hydrologic warming [*Phillips et al*., 2013].

Firn aquifers are important sites for storage of the increased melt observed in Greenland. In the percolation zone of West Greenland, *Harper et al*. [2012] reported available pore space in the firn being filled with meltwater that refreezes, leading to an increased number of ice lenses, until capacity is reached. Recent observations, in a similar region [*Machguth et al*., 2016], suggested that formation of near-surface thick ice layers renders pore space at depth inaccessible during intense melt years (i.e., 2012), promoting early runoff. For the aquifer at our Ridgeline site, however, even if we observe surface lowering, we did not observe a substantial interannual increase in ice fraction in the snow/firn column above the water table, not even after the warm summer of 2012. If the additional meltwater is not contributing to an increase in the ice fraction of the firn above the water table by refreezing, then this implies that there is slow runoff of the water at depth under low hydraulic gradient year-round. However, our ice-fraction observations are spatially limited (four firn cores only), and in places where water is close to the snow surface (less than 10 m), we suspect that freezing would occur from top-down as the cold wave penetrates at depth during winter. The fate of the water drained from the firn aquifer is not clear from the radar data set only. In crevassed areas, the absence of bright reflectors in radar profiles suggests that the water could have drained into the crevasses either refreezing or finding englacial pathways toward the glacier bed. On mountain glaciers, the firn aquifer is intimately linked to the englacial network via crevasses and moulins [*Fountain and Walder*, 1998], allowing meltwater to access the bed after being delayed in the aquifer. In Greenland, englacial pathways from the surface to the bed have been inferred [e.g., *Catania and Neumann*, 2010]; however, there are no observations yet of meltwater exiting the aquifer to reach the bed. The consequences of delaying or suppressing meltwater flow to the bed can be related to seasonal changes in glacier velocity in Southeast Greenland [*Moon et al*., 2014]. For the studied aquifer location, the ice thickness is $>$800 m and the formation of moulins, necessary for bringing water to greater depths, depends on the water amount and rate. Indeed, to bring aquifer water to the bed, enough

water would need to flow at a high rate to keep up with the crevasse penetration rate [e.g., *van der Veen*, 2007]. However, an initial modeling effort using similar flow rates to the ones calculated in section 6.6 shows that the aquifer can release sufficient water into downstream crevasses for fractures to propagate to the bed [*McNerney*, 2016].

8. Conclusions

Widespread firn aquifers have been detected directly or inferred over high accumulation regions of the Greenland ice sheet by a variety of radars systems: a 195 MHz radar depth sounder, a 750 MHz accumulation radar (AR), and a 400 MHz ground-penetrating radar. A total linear distance of 3930 km of firn aquifers, inferred to represent a total area of 21,900 km^2, has been observed and mapped using the AR between spring 2010 and spring 2014 in the lower part of the percolation zone (wet-snow zone). The firn aquifers are mainly observed in the southeast and south sectors of the ice sheet, representing an area of 17,920 km^2. Firn aquifers are found at an average elevation of 1615 ± 300 m ($\pm 1\sigma$), an average accumulation rate of 1.0 ± 0.4 m w.e. yr^{-1} ($\pm 1\sigma$), and the average depth to the water table (top of the aquifer) is 22 ± 7 m ($\pm 1\sigma$). Driven by low hydraulic gradients (0.01), water in the aquifer flows downglacier following ice sheet surface undulations. Within the firn aquifer, local flow cells are simulated and their lateral limits are related to the surface topography with water discharge located at the steep-to-flat transitions. The firn-aquifer observed upstream of Helheim Glacier responds to the recent above-average melt years and is expanding toward the ice sheet interior. We also observed drainage of its lower elevation portion between spring 2012 and spring 2013. The movement of meltwater from the aquifer into nearby crevasses would warm the ice in the vicinity by refreezing and releasing latent heat. If the amount of water draining out of the aquifer into a crevasse is sufficient for hydrofracturing, the water could reach the bed, influencing ice dynamics. To further our understanding of firn-aquifer drainage, we recommend modeling work joint with water discharge measurements to characterize these englacial pathways and subglacial connections. Regarding firn-aquifer formation and evolution, we also recommend additional field observations to better constrain both the hydraulic variables (hydraulic conductivity, water age, and residence time) and the water volume mobilized in the aquifer. Although many firn-aquifer effects on the ice sheet still need to be further characterized, we have shown that firn aquifers are extensive features covering a substantial portion of the ice sheet percolation zone. They are long-lived, dynamic systems responding to surface melt variations that will likely increase and play a more significant role in future warmer climate scenarios.

Acknowledgments

We would like to thank Scientific Editor Bryn Hubbard for handling our manuscript and for his comments, as well as an Associate Editor, three anonymous reviewers and Jack Kohler for many insights and suggestions that substantially improved this manuscript. Thanks to NASA Operation IceBridge and CReSIS at the University of Kansas for the high-quality airborne data that made this study possible. CReSIS data were generated with support from NSF (ANT-0424589) and NASA (NNX13AD53A). C. Miège acknowledges NASA ESS Fellowship program (NNX11AL64H). NSF with grants OPP-0909499 and EAGER-1311655 supported fieldwork in 2011 and 2013. L. Brucker and L. Koenig were supported by NASA's Cryospheric Science Program. R. Forster acknowledges NASA grant NNX13AK23G. J. Box and R. Fausto are supported by the Det Frie Forskningsråd of Denmark grant DFF–4002-00234. Thanks to the 2011 and 2013 field team members: B. Ballard, T. Gacke, and J. Kyne. Thanks to the following institutions for the fieldwork support: CH2MHILL, IDDO, 109th Air National Guard, Air Greenland, and UNAVCO. Thanks to G. Roth at the Polar Geospatial Center for preparing the DigitalGlobe© images. Thanks to J. Collins at CReSIS for the careful grammatical edits on this manuscript. Thanks to Xavier Fettweis at the University of Liège for the availability of his MAR output data. The firn-aquifer map and depth to the water table are available for download at nsidc.org/acadis or by contacting the lead author (clement.miege@geog.utah.edu).

References

Ahlstrøm, A. P., and the PROMICE project team (2008), A new programme for monitoring the mass loss of the Greenland ice sheet, Review of Survey activities 2007, *Geol. Surv. Den. Greenl. Bull.*, *15*, 61-–64.

Benson, C. S. (1962), Stratigraphic studies in the snow and firn of the Greenland ice sheet, *CRREL Res. Rep. 70*.

Bradford, J. H., J. T. Harper, and J. Brown (2009), Complex dielectric permittivity measurements from ground-penetrating radar data to estimate snow liquid water content in the pendular regime, *Water Resour. Res.*, *45*, W08403, doi:10.1029/2008WR007341.

Burgess, E. W., R. R. Forster, J. E. Box, E. Mosley-Thompson, D. H. Bromwich, R. C. Bales, and L. C. Smith (2010), A spatially calibrated model of annual accumulation rate on the Greenland ice sheet (1958–2007), *J. Geophys. Res.*, *115*, F02004, doi:10.1029/2009JF001293.

Catania, G. A., and T. A. Neumann (2010), Persistent englacial drainage features in the Greenland Ice Sheet, *Geophys. Res. Lett.*, *37*(2), L02501, doi:10.1029/2009GL041108.

Christianson, K., J. Kohler, R. B. Alley, C. Nuth, and W. J. J. van Pelt (2015), Dynamic perennial firn aquifer on an Arctic glacier, *Geophys. Res. Lett.*, *42*, 1418–1426, doi:10.1002/2014GL062806.

Colbeck, S. C. (1975), A theory for water flow through a layered snowpack, *Water Resour. Res.*, *11*, 261–266, doi:10.1029/WR011i002p00261.

Coléou, C., and B. Lesaffre (1998), Irreducible water saturation in snow: Experimental results in a cold laboratory, *Ann. Glaciol.*, *26*, 64–68.

Conway, H., and R. Benedict (1994), Infiltration of water into snow, *Water Resour. Res.*, *30*, 641–649, doi:10.1029/93WR03247.

Enderlin, E. M., I. M. Howat, S. Jeong, M.-J. Noh, J. H. van Angelen, and M. R. van den Broeke (2014), An improved mass budget for the Greenland ice sheet, *Geophys. Res. Lett.*, *41*, 866–872, doi:10.1002/2013GL059010.

Fettweis, X., B. Franco, M. Tedesco, J. H. van Angelen, J. T. M. Lenaerts, M. R. van den Broeke, and H. Gallée (2013), Estimating the Greenland ice sheet surface mass balance contribution to future sea level rise using the regional atmospheric climate model MAR, *Cryosphere*, *7*(2), 469–489, doi:10.5194/tc-7-469-2013.

Forster, R. R., et al. (2014), Extensive liquid meltwater storage in firn within the Greenland ice sheet, *Nat. Geosci.*, *7*(2), 95–98, doi:10.1038/ngeo2043.

Fountain, A. G. (1989), The storage of water in, and hydraulic characteristics of, the firn of South Cascade Glacier, Washington State, U.S.A., *Ann. Glaciol.*, *13*, 69–75.

Fountain, A. G. (1996), Effect of snow and firn hydrology on the physical and chemical characteristics of glacial runoff, *Hydrol. Processes*, *10*(4), 509–521.

Fountain, A. G., and J. S. Walder (1998), Water flow through temperate glaciers, *Rev. Geophys.*, *36*, 299–328, doi:10.1029/97RG03579.

Gascon, G., M. Sharp, D. Burgess, P. Bezeau, and A. B. G. Bush (2013), Changes in accumulation-area firn stratigraphy and meltwater flow during a period of climate warming: Devon Ice Cap, Nunavut, Canada, *J. Geophys. Res. Earth Surf.*, *118*, 2380–2391, doi:10.1002/2013JF002838.

Harper, J., N. Humphrey, W. T. Pfeffer, J. Brown, and X. Fettweis (2012), Greenland ice-sheet contribution to sea-level rise buffered by meltwater storage in firn, *Nature*, *491*(7423), 240–243, doi:10.1038/nature11566.

Helm, V., A. Humbert, and H. Miller (2014), Elevation and elevation change of Greenland and Antarctica derived from CryoSat-2, *Cryosphere*, *8*(4), 1539–1559, doi:10.5194/tc-8-1539-2014.

Howat, I. M., A. Negrete, and B. E. Smith (2014), The Greenland Ice Mapping Project (GIMP) land classification and surface elevation data sets, *Cryosphere*, *8*(4), 1509–1518, doi:10.5194/tc-8-1509-2014.

Humphrey, N. F., J. T. Harper, and W. T. Pfeffer (2012), Thermal tracking of meltwater retention in Greenland's accumulation area, *J. Geophys. Res.*, *117*, F01010, doi:10.1029/2011JF002083.

Jansson, P., R. Hock, and T. Schneider (2003), The concept of glacier storage: A review, *J. Hydrol.*, *282*(1–4), 116–129, doi:10.1016/S0022-1694(03)00258-0.

Jones, N. L. (1999), SEEP2D Primer, Environ. Model. Res. Lab., Brigham Young Univ., Provo, Utah.

Koenig, L. S., C. Miège, R. R. Forster, and L. Brucker (2014), Initial in situ measurements of perennial meltwater storage in the Greenland firn aquifer, *Geophys. Res. Lett.*, *41*, 81–85, doi:10.1002/2013GL058083.

Kovacs, A., A. J. Gow, and R. M. Morey (1995), The in-situ dielectric constant of polar firn revisited, *Cold Reg. Sci. Technol.*, *23*(3), 245–256, doi:10.1016/0165-232X(94)00016-Q.

Krabill, W. B. (2013), IceBridge ATM L2 Icessn Elevation, Slope, and Roughness, version 2 [2010–2014], NASA DAAC at the Natl. Snow and Ice Data Cent., Boulder, Colo.

Krabill, W. B., W. Abdalati, E. B. Frederick, S. S. Manizade, C. F. Martin, J. G. Sonntag, R. N. Swift, R. H. Thomas, and J. G. Yungel (2002), Aircraft laser altimetry measurement of elevation changes of the Greenland ice sheet: Technique and accuracy assessment, *J. Geodyn.*, *34*(3–4), 357–376, doi:10.1016/S0264-3707(02)00040-6.

Kuipers Munneke, P., S. R. M. Ligtenberg, M. R. van den Broeke, J. H. van Angelen, and R. R. Forster (2014), Explaining the presence of perennial liquid water bodies in the firn of the Greenland ice sheet, *Geophys. Res. Lett.*, *41*, 476–483, doi:10.1002/2013GL058389.

Leuschen, C., C. Lewis, P. Gogineni, F. Rodriguez-Morales, J. Paden, and J. Li (2014a), IceBridge accumulation radar L1B geolocated radar echo strength profiles, version 2 [2010–2014], NASA DAAC at the Natl. Snow and Ice Data Cent., Boulder, Colo.

Leuschen, C., P. Gogineni, R. Hale, J. Paden, F. Rodriguez-Morales, B. Panzer, and D. Gomez (2014b), IceBridge MCoRDS L1B geolocated radar echo strength profiles, version 2 [2010–2014], NASA DAAC at the Natl. Snow and Ice Data Cent., Boulder, Colo.

Machguth, H., M. MacFerrin, D. van As, J. E. Box, C. Charalampidis, W. Colgan, R. S. Fausto, H. A. J. Meijer, E. Mosley-Thompson, and R. S. W. van de Wal (2016), Greenland meltwater storage in firn limited by near-surface ice formation, *Nat. Clim. Change*, *6*, 390–393, doi:10.1038/nclimate2899.

McGrath, D., W. Colgan, N. Bayou, A. Muto, and K. Steffen (2013), Recent warming at Summit, Greenland: Global context and implications, *Geophys. Res. Lett.*, *40*, 2091–2096, doi:10.1002/grl.50456.

McNerney, L. (2016), Constraining the Greenland firn aquifer's ability to hydrofracture a crevasse to the bed of the ice sheet, pp. 1–54 .

Miège, C., R. R. Forster, J. E. Box, E. W. Burgess, J. R. McConnell, D. R. Pasteris, and V. B. Spikes (2013), Southeast Greenland high accumulation rates derived from firn cores and ground-penetrating radar, *Ann. Glaciol.*, *54*(63), 322–332, doi:10.3189/2013AoG63A358.

Moon, T., and I. Joughin (2008), Changes in ice front position on Greenland's outlet glaciers from 1992 to 2007, *J. Geophys. Res.*, *113*, F02022, doi:10.1029/2007JF000927.

Moon, T., I. Joughin, B. Smith, M. R. van den Broeke, W. J. van de Berg, B. Noël, and M. Usher (2014), Distinct patterns of seasonal Greenland glacier velocity, *Geophys. Res. Lett.*, *41*, 7209–7216, doi:10.1002/2014GL061836.

Oerter, H., and H. Moser (1982), Water storage and drainage within the firn of a temperate glacier (Vernagtferner, Oetztal Alps, Austria), in *Hydrological Aspects of Alpine and High-Mountain Areas*, Proceedings of the Exeter Symposium, vol. 138, pp. 71–81, IAHS Publ. no. 138.

Pfeffer, W. T., and N. F. Humphrey (1996), Determination of timing and location of water movement and ice-layer formation by temperature measurements in sub-freezing snow, *J. Glaciol.*, *42*(141), 292–304.

Phillips, T., H. Rajaram, W. Colgan, K. Steffen, and W. Abdalati (2013), Evaluation of cryo-hydrologic warming as an explanation for increased ice velocities in the wet snow zone, Sermeq Avannarleq, West Greenland, *J. Geophys. Res. Earth Surf.*, *118*, 1241–1256, doi:10.1002/jgrf.20079.

Raymond, C. F., and K. Tusima (1979), Grain coarsening of water-saturated snow, *J. Glaciol.*, *22*, 83–105.

Rignot, E., and J. Mouginot (2012), Ice flow in Greenland for the International Polar Year 2008–2009, *Geophys. Res. Lett.*, *39*, L11501, doi:10.1029/2012GL051634.

Rignot, E., I. Velicogna, M. R. van den Broeke, A. Monaghan, and J. T. M. Lenaerts (2011), Acceleration of the contribution of the Greenland and Antarctic ice sheets to sea level rise, *Geophys. Res. Lett.*, *38*, L05503, doi:10.1029/2011GL046583.

Rodriguez-Morales, F., et al. (2013), Advanced multifrequency radar instrumentation for polar research, *IEEE Trans. Geosci. Remote Sens.*, *52*, 2824–2842, doi:10.1109/TGRS.2013.2266415.

Schneider, T. (1999), Water movement in the firn of Storglaciaren, Sweden, *J. Glaciol.*, *45*(150), 286–294.

Schneider, T., and P. Jansson (2004), Internal accumulation in firn and its significance for the mass balance of Storglaciären, Sweden, *J. Glaciol.*, *50*(168), 25–34, doi:10.3189/172756504781830277.

Smith, B. M., and S. Evans (1972), Radio echo sounding: Absorption and scattering by water inclusion and ice lenses, *J. Glaciol.*, *11*, 133–146.

Spikes, V. B., G. S. Hamilton, S. A. Arcone, S. Kaspari, and P. A. Mayewski (2004), Variability in accumulation rates from GPR profiling on the West Antarctic plateau, *Ann. Glaciol.*, *39*(1), 238–244, doi:10.3189/172756404781814393.

Tedesco, M., X. Fettweis, T. Mote, J. Wahr, P. Alexander, J. E. Box, and B. Wouters (2013), Evidence and analysis of 2012 Greenland records from spaceborne observations, a regional climate model and reanalysis data, *Cryosphere*, *7*(2), 615–630, doi:10.5194/tc-7-615-2013.

Tóth, J. (1963), A theoretical analysis of groundwater flow in small drainage basins, *J. Geophys. Res.*, *68*, 4795–4812, doi:10.1029/JZ068i016p04795.

van der Veen, C. J. (2007), Fracture propagation as means of rapidly transferring surface meltwater to the base of glaciers, *Geophys. Res. Lett.*, *34*, L01501, doi:10.1029/2006GL028385.